MOLECULAR AND CELLULAR BIOLOGY, Feb. 2011, p. 756–765 Vol. 31, No. 4
0270-7306/11/$12.00 doi:10.1128/MCB.00811-10

Tumor Necrosis Factor Alpha and Inflammation Disrupt the Polarity Complex in Intestinal Epithelial Cells by a Posttranslational Mechanism[▽]

Anastasia Mashukova, Flavia A. Wald, and Pedro J. Salas*

University of Miami, Miller School of Medicine, Department of Cell Biology, Miami, Florida 33186

Received 14 July 2010/Returned for modification 1 October 2010/Accepted 26 November 2010

Inflammatory processes disrupt the barrier function in epithelia. Increased permeability often leads to chronic of inflammation. Important among other cytokines, tumor necrosis factor alpha (TNF-α) initiates an NF-κB-mediated response that leads to upregulation of myosin light chain kinase (MLCK), a hallmark of the pathogenesis of inflammatory bowel disease. Here, we found that two components of the evolutionarily conserved organizer of tight junctions and polarity, the polarity complex (atypical protein kinase C [aPKC]-PAR6-PAR3) were downregulated by TNF-α signaling in intestinal epithelial cells and also *in vivo* during intestinal inflammation. Decreases in aPKC levels were due to decreased chaperoning activity of Hsp70 proteins, with failure of the aPKC rescue machinery, and these effects were rescued by NF-κB inhibition. Comparable downregulation of aPKC shRNA phenocopied effects of TNF-α signaling, including apical nonmuscle myosin II accumulation and myosin light chain phosphorylation. These effects, including ZO-1 downregulation, were rescued by overexpression of constitutively active aPKC. We conclude that this novel mechanism is a complementary effector pathway for TNF-α signaling.

Loss of tight junction (TJ) competence is an important pathophysiological mechanism in inflammatory bowel disease (IBD) for both epithelium and endothelium (6, 29), blood-brain barrier breakdown in ischemic stroke (39), and in airway epithelium dysfunction in asthma (17). Increased TJ permeability facilitates the diffusion of small antigens and bacterial toxins, which in turn can exacerbate or perpetuate the inflammatory process (8, 29). Cytokines initiate proinflammatory signaling on intestinal epithelial cells in IBD, including tumor necrosis factor alpha (TNF-α), gamma interferon (IFN-γ), and several interleukins (1, 28, 29). Remarkably, the first two cytokines induce sharp increases in TJ permeability independently of apoptosis (5). TNF-α alone can reduce electrical resistance in intestinal epithelial cells in culture (26). However, the molecular mechanisms downstream of proinflammatory signaling remain unclear. Some aspects of the cellular responses to TNF-α and IFN-γ on the epithelial barrier that have been identified include endocytosis of TJ components, changes in actin-myosin complexes (21), and downregulation of claudins (2). Activation of the myosin light chain (MLC) due to upregulation of myosin light chain kinase (MLCK) has been reported by several groups as the final effector of proinflammatory signaling in epithelial cells and an essential player in tight junction organization (25, 44, 50). The implication of MLCK upregulation is that an increase in nonmuscle myosin II (nmMII) assembly mediates the effects of proinflammatory signaling in simple epithelia. However, little is known about the myosin heavy chains involved. A mounting body of evidence suggests that nmMII heavy chain type A (nmMIIA; MYH9), but not type B (MYH10) or type C (MYH14) isoforms, is important for the organization of tight junctions (20, 46).

However, there is a striking disconnection between the studies mentioned above and a large body of work that has identified partition-deficient (PAR) mutants in *Caenorhabditis elegans* (37). Those studies provided overwhelming evidence for the role of the PAR3-PAR6 polarity complex with atypical protein kinase C (aPKC; namely, PKCι/λ and PKCζ isoforms) as the evolutionarily conserved organizer of polarity and TJ assembly in epithelial cells (15, 41, 42). Expression of dominant negative aPKC in epithelial cells results in TJ proteins (ZO-1, occludin, and claudins) that are localized at the cell surface in clusters but not in the typical belt-like structure around the apical domain (32, 43). Importantly, suppression of ZO-1, ZO-2, and ZO-3 abrogates the formation of TJs but does not affect the localization or activity of aPKC (19, 45), indicating that aPKC is "upstream" of TJ formation.

The catalytic domains of all PKC isoforms require a specific conformation, with PDK-1-mediated phosphorylation in the activation domain (T410 in hPKCι) followed by autophosphorylation in the turn domain (T555 in hPKCι) (16). The catalytic domain becomes dephosphorylated and loses the active conformation as a consequence of its own kinase activity. Dephosphorylated PKCs are then ubiquitinylated and degraded (34). This feature of PKCs has been used to downregulate conventional isoforms by prolongued exposure to activating phorbol esters (22). It is widely accepted that a substantial fraction of dephosphorylated PKC can be rescued by Hsp/Hsc70-mediated refolding followed by rephosphorylation of the activation and turn motifs (14). In epithelial cells, the rescue of aPKC is dependent on a small subset of Hsp/Hsc70 proteins that operate on a cytoskeletal intermediate filament (IF) scaffold which is responsible for the maintenance of normal steady-state lev-

* Corresponding author. Mailing address: University of Miami, Miller School of Medicine, Department of Cell Biology, R-124, RMSB, 1600 NW 10th Ave., Miami, FL 33136. Phone: (305) 243-6977. Fax: (305) 545-7166. E-mail: psalas@miami.edu.

▽ Published ahead of print on 6 December 2010.

els of aPKC. Those levels decrease more than 90% if any of the components of the chaperone/keratin machinery is knocked down (30).

Hsp70 proteins are downregulated under synergistic TNF-α and IFN-γ proinflammatory signaling via a translational control (18). Bearing in mind the rescue mechanism of aPKC by Hsp70 proteins and the fact that PKC activity is important in the regulation of myosin II assembly (47), we hypothesized that active aPKC levels may decrease during inflammation, thus becoming an additional molecular mechanism for the disruption of epithelial function.

MATERIALS AND METHODS

Cell culture, Caco-2 cell lentiviral infection, extraction, and fractionation. Caco-2 cells and the C2BBe clone were obtained from the American Type Culture Collection and cultured as described previously (48). PKCι shRNA (CCGGGCCTGG ATACAATTAA CCATTCTCGA GAATGGTTA ATTGT ATCCA GGCTTTTT) was obtained from Open Biosystems (clone number TRCN0000006037) in the pLKO.1 lentivirus vector. Lentiviral packaging of the vector was performed as described earlier (48). Caco-2 cells were typically infected at 2 days after seeding and selected in 5 μg/ml puromycin for 10 days. Constitutively active PKCι (A120E) was amplified from the mutated full-length cDNA construct in a pcDNA3.1/V5-His TOPO vector, which has been described previously (48). Amplified mutated cDNA was subcloned into a pLenti6.2/V5-DEST vector (Invitrogen) according to the manufacturer's specifications and confirmed to be correct by PCR sequencing of the full-length open reading frame. Lentiviral packaging was done using the ViraPower lentiviral expression system from Invitrogen. Caco-2 cells were typically infected 2 days after seeding and selected with blasticidin (20 μg/ml) for 10 to 14 days.

The cell extraction procedure has been described elsewhere (30). Briefly, at 10 days after seeding, cells were extracted in phosphate-buffered saline (PBS) containing 1% Triton X-100, 1 mM EDTA supplemented with cocktails of protease and phosphatase inhibitors at room temperature. After three 5-s intervals of sonication, the cell extract was spun for 10 min at 16,000 × *g*. This first supernatant is referred to as the S1 fraction. The pellet was resuspended in 1.5 M KCl, sonicated for 15 s (three intervals), incubated for 10 min on ice, and spun for 10 min at 16,000 × *g*. The resulting supernatant is referred to as the S2 fraction, and the pellet is referred to as the P fraction.

Apoptosis detection. A positive control for apoptosis was included by incubating Caco-2 cells in 30 mM H_2O_2 for 2 h. Following the incubation, apoptosis levels were assessed using the Apoptotic DNA Ladder kit (Roche) according to the manufacturer's instructions and by immunoblot analysis to determine caspase-3 cleavage.

PKCι rephosphorylation. The method for analysis of PKCι rephosphorylation in the soluble fraction of Caco-2 cells has been described elsewhere (30). Briefly, untreated Caco-2 cells or Caco-2 cells treated with 10 ng/ml TNF-α overnight were fractionated (S1, S2, and P) as described above, with the exception that the extraction buffer was not supplemented with phosphatase inhibitors. To induce the activity-dependent dephosphorylation of aPKC, the S1 and P fractions were incubated in the presence of 150 μM PKC substrate peptide (Upstate Biotechnology) and 1 mM ATP at 30°C with gentle shaking for 5 h. After treatment, the peptide was removed by ultrafiltration. To measure aPKC rephosphorylation, 50 μg of S1 fraction protein was then incubated with 20 μg of the P fraction protein or with 15 μg of purified IFs (40) from Caco-2 cells in the presence or absence of 1 mM ATP at 30°C for 4 h. The phosphorylation state of PKCι was examined by Western blotting with anti-pT555-PKCι antibodies. Statistical analyses of band intensity differences in the immunoblot assays were done by using Student's *t* test.

Metabolic labeling and immunoprecipitation. For metabolic labeling, 10-day-old Caco-2 cells treated or not with 10 ng/ml TNF-α overnight were incubated in Dulbecco's modified Eagle's medium (DMEM) without cysteine and methionine for 45 min and then supplemented with 0.7 mCi/ml [^{35}S]methionine/cysteine (Perkin-Elmer, Boston, MA) in the presence of 0.1 mM cold methionine/cysteine for 1 h 30 min from the basolateral side. It takes approximately 45 min for the label to diffuse through the filters. The chase was initiated by washes in regular DMEM. The cells were extracted as described above for S1. Immunoprecipitation was done as described previously (30). For autoradiography, samples were run on an SDS-PAGE gel, blotted, and analyzed with a phosphorimager.

Transepithelial electrical resistance. The cells were seeded on Snapwell filters and measured in Ussing chambers using Ag-AgCl electrodes and 3 M KCl agar bridges. The electrical resistance was measured in air-vented standard Ringer solution at 37°C with a Physiologic Instruments VCC MC6 voltage-clamp instrument.

Luciferase folding assay. Refolding of chemically denatured firefly luciferase was carried out as described previously (24).

PKC and PDK-1 activity assay kits were from Assay Designs and CycLex Co., Ltd., respectively. Relative kinase activity was normalized per μg of protein.

Animal studies, transgenic mice, and analyses of intestinal epithelium. Studies of animals were performed in compliance with regulations of the Office of Laboratory Animal Welfare (OLAW), National Institutes of Health, and monitored by an internal Animal Care and Use Committee. The Hsp70-null transgenic mice were obtained from the Mutant Mouse Regional Resource Centers (MMRRC) network (http://www.mmrrc.org/) and are referenced as Hspa1a/Hspa1btm1Dix. For dextran-sulfate sodium (DSS) treatment, the animals were provided a 5% DSS solution in the drinking water and allowed to drink *ad libitum*. The disease activity index (DAI) was estimated as described previously (10) and monitored daily during DSS treatment. Animals were euthanized when their DAI reached ≥3 (the maximum index is 4). Procedures for intestinal cell isolation have been described before (30) and included EDTA dissociation with approximately 70% enrichment of epithelial cells.

Immunofluorescence. All images were collected with a Leica DM microscope using a 63× (1.4-numerical aperture) oil immersion objective. Confocal images were collected with a Leica SP5 confocal microscope, typically at Airy 0.8 (0.6-μm optical sections) with the same optics. Confocal stacks were collected at 0.1- by 0.1- by 0.4-μm voxel size. Three-dimensional reconstructions of confocal stacks were performed using SlideBook software from seven-voxel-deep cross-sections of a confocal stack.

qPCR. RNA for quantitative PCR (qPCR) was extracted using an RNeasy minikit from Qiagen according to the manufacturer's specifications. qPCR was performed at the Qiagen facility.

Statistics. In all cases, variables were normally distributed. Significance of differences between pairs of average values were determined with Student's *t* test.

RESULTS

TNF-α and inflammation downregulate PKCι and aPKC activities *in vitro* and *in vivo*. To study the effects of proinflammatory signaling on aPKC, we used human colon carcinoma (Caco-2) cells grown on filters; these cells differentiate and polarize in culture similar to enterocytes (36).The medium on the basolateral side was supplemented with TNF-α (1 or 10 ng/ml) to mimic inflammatory signaling. Although other cytokines are also present in colitis, we focused on this specific cytokine because anti-TNF-α antibodies are clinically effective in the treatment of chronic colitis (13). These TNF-α levels are well within the range of concentrations in the human intestinal mucosa in IBD (35) and the concentrations known to cause a maximal decrease in TJ permeability (26). For *in vivo* studies, we used acute inflammation induced by DSS, which has been validated as a relevant model for human bowel inflammation (31). In Caco-2 cells, TNF-α applied basolaterally to the cells resulted in a 74% decrease in total PKCι protein (Fig. 1A and B). PKC kinase activity was measured in a Triton X-100-soluble fraction (S1), a Triton-insoluble, 1.5 M KCl-soluble fraction (S2; mostly actin cytoskeleton), and the final pellet (P; mostly the IF cytoskeleton), all of which have been described before (30). Activities of conventional and atypical PKCs were distinguished by using specific inhibitors (GF10923X and a highly specific aPKC pseudosubstrate peptide). In the S1 fraction, TNF-α stimulation caused a nonsignificant decrease in total PKC activity. This fraction, however, contains all PKC isoforms. aPKC is enriched in the S2 fraction and represents most of the PKC activity in the P fraction (30). When these two fractions were tested, a significant decrease in PKC activity was observed in the TNF-α-treated cells. Importantly, this signifi-

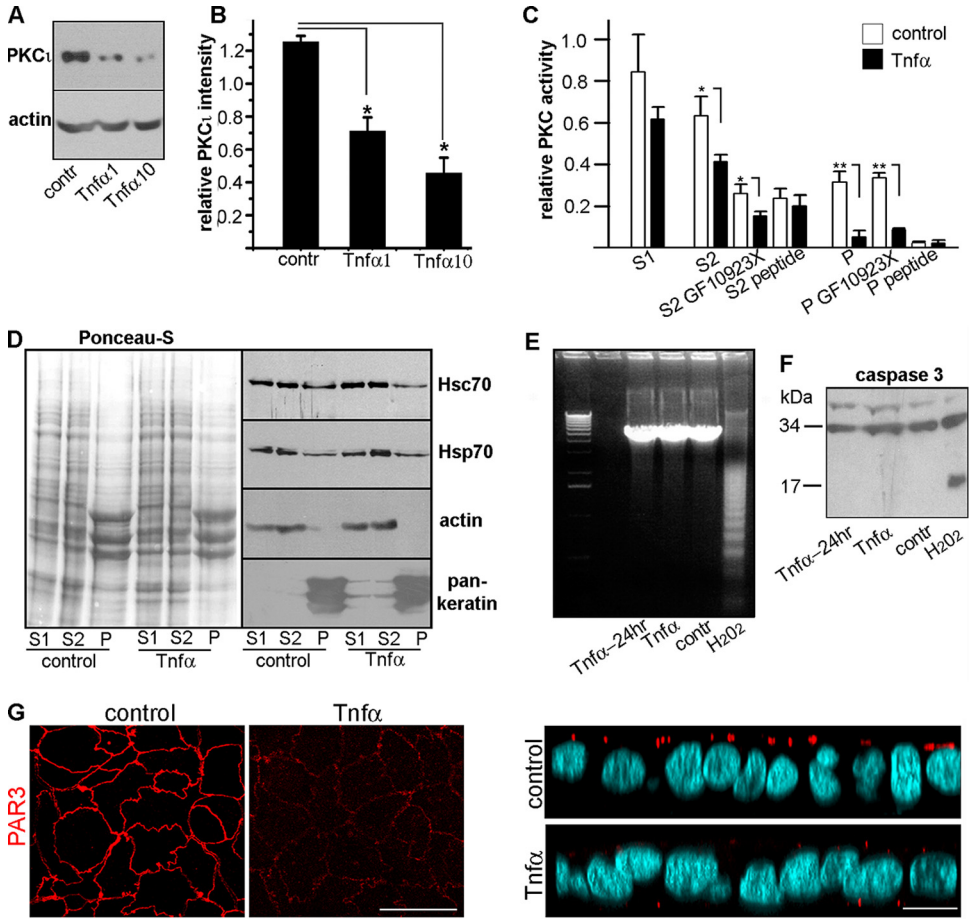

FIG. 1. TNF-α downregulates PKCι in Caco-2 cells in the absence of apoptosis. (A) Confluent polarized Caco-2 cells cultured on filters were incubated overnight with 0 (contr), 1 ng/ml TNF-α (1), or 10 ng/ml TNF-α (10) applied from the basolateral side only. Following the treatment, total SDS cell extracts were analyzed by immunoblotting. (B) The relative PKCι intensity was calculated as the ratio of PKCι to actin band densities. The means ± SD from three independent experiments are shown. *, $P < 0.025$. (C) Caco-2 cells were incubated with 0 or 10 ng/ml TNF-α overnight and fractionated in the S1 (Triton X-100-soluble supernatant), S2 (1.5 M KCl supernatant), and P (intermediate filament cytoskeleton) fractions as described previously (30). Each fraction was assayed for PKC kinase activity alone or when supplemented with either 1 μM GF10923X (inhibiting conventional and novel PKCs) or 50 μM aPKC pseudosubstrate peptide (specifically inhibiting PKCι and -ζ). Kinase activity per μg of protein is shown as the average ± the SD ($n = 3$). *, $P < 0.001$. (D) TNF-α does not affect the amount or distribution of Hsp/Hsc70 proteins in Caco-2 cells. Caco-2 cells were incubated overnight with 0 (control) or 10 ng/ml TNF-α and separated into S1, S2, and P fractions. The total protein load (Ponceau-S) and the immunoblots for Hsp70, Hsc70, actin, and keratins are shown (50 μg protein/lane). (E and F) The lack of apoptosis was controlled in a DNA laddering assay (E) and via caspase-3 degradation (F) in cells incubated in 0 (contr) or 10 ng/ml TNF-α for 24 h (Tnfα-24hr) or overnight (Tnfα). As a positive control for apoptosis, the cells were incubated in 30 mM H_2O_2 for 2 h. (G) Confocal sections of Caco-2 cells cultured and treated with 10 ng/ml TNF-α or not, as described above. The cells were processed with anti-PAR3 antibody (red channel) and counterstained with DAPI (light blue). The left panels show the *x-y* confocal sections at the apical level, and the right panels show *x-z* sections of the same stacks. Bars, 10 μm.

cant difference was poorly (S2) or not at all (P) affected by GF10923X but was abrogated by the aPKC pseudosubstrate inhibitor peptide in the P fraction (Fig. 1C). This result indicated that the effect of TNF-α is selective for aPKC.

We also determined the levels of Hsp70 proteins Hsc70 (Hsp70 cognate protein 8, constitutive) and Hsp70 (Hsp70.1, heat shock inducible) in TNF-α-treated cells and controls fractionated into S1, S2, and P. Consistent with previous results showing the need for TNF-α along with IFN-γ (18), we found no change in the heat shock protein levels in the presence of TNF-α alone (Fig. 1D). Importantly, the highest dose of TNF-α used in these studies did not cause apoptosis, not even with longer exposure times (24 h), as determined by DNA laddering and caspase-3 cleavage (Fig. 1E and F). To assess if other components of the polarity complex were also affected by TNF-α signaling, we studied PAR3 immunofluorescence signals in confocal images under identical gain conditions. Only vestigial PAR3 signal was observed after TNF-α treatment (Fig. 1G).

To validate the previous results in the more complex inflammatory environment in an animal model, in which various cytokines act simultaneously, DSS-induced colitis was standardized to euthanize the animals as soon as the multiparameter DAI (which accounts for weight loss and anal bleeding) reached 3 (5 to 8 days of treatment). Substantial mucosal inflammatory infiltration was observed in the colon compared to controls (Fig. 2A and B, arrows). In control mice, active aPKC (pT555-aPKC) was localized to the TJ region in colon

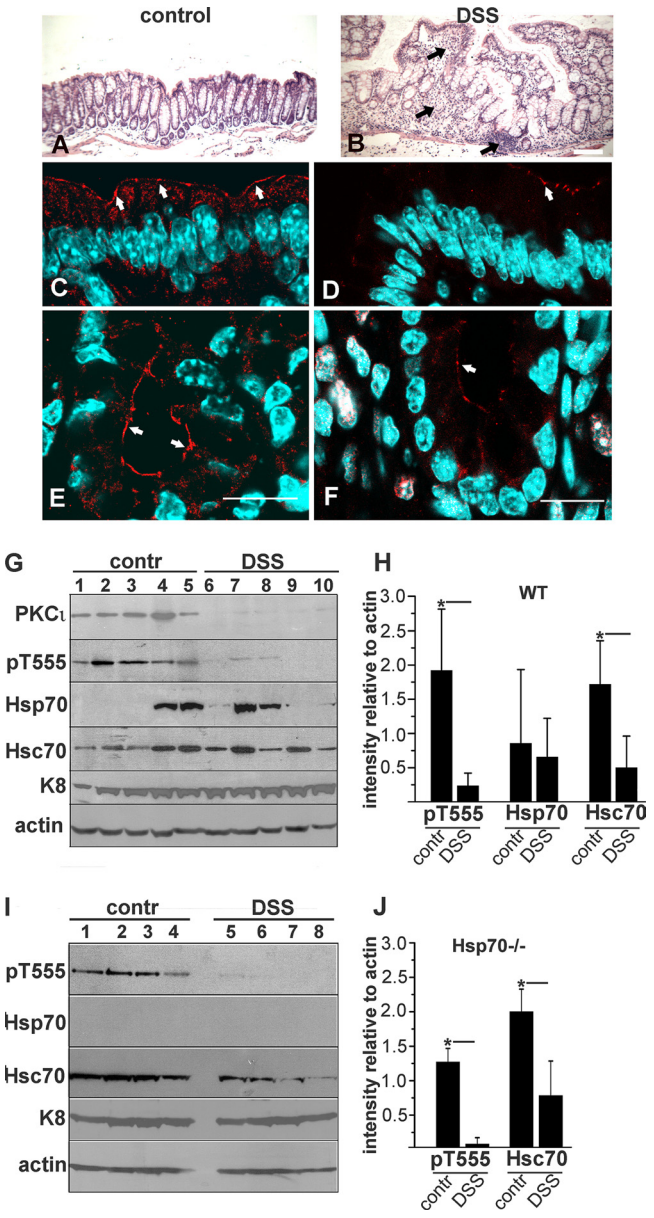

FIG. 2. Downregulation of aPKC in the large intestine upon DSS-induced inflammation. (A to F) FVBn wild-type mice were treated with DSS and sacrificed when the DAI was ≥3, usually after 5 to 8 days of treatment (B, D, and F). Control animals were kept under the same conditions (A, C, and E). Adjacent pieces of colon within 1 cm from the ileocecal valve were processed for hematoxylin and eosin staining (A and B, black arrows indicate inflammatory infiltration of the lamina propria) or fixed, frozen, and stained for immunofluorescence with anti-pT555 aPKC antibody (red) and counterstained with DAPI (light blue). Single confocal sections are shown (C to F), and the arrows point to apical aPKC. Bars: 100 μm (A and B) or 20 μm (C to F). (G) Immunoblots from enterocytes. Lanes 1 to 5, control animals; lanes 6 to 10, DSS-treated animals. (I) An identical experiment was performed using C57BL/6 × 129S7 Hsp70a/Hsp70b-null mice. (H and J) Band intensities relative to actin were quantified in the experiments in G and I and are shown as averages ± SD. *, $P < 0.05$.

surface epithelium (Fig. 2C, arrows) and to the entire apical region in the crypts (Fig. 2E, arrows), similar to previous observations in the small intestine (30, 48). This distribution mostly disappeared in both areas in the DSS-treated mice, and only a few cells showed vestigial aPKC signal (Fig. 2D and F, arrows). The chromatin visualized by using 4′,6-diamidino-2-phenylindole (DAPI) did not show any morphological sign of apoptosis in the same cells. An identical result was semiquantitatively confirmed by immunoblotting of total protein from purified colon epithelial cells. In these experiments we found a significant 87% decrease in the active T555-phosphorylated form of aPKC, as well as in total aPKC protein level (Fig. 2G and H).

Because we and others have shown that aPKC levels are sustained by a continuous rescue mediated by Hsp70/Hsc70 and the cytoskeleton (16, 30), we analyzed the expression of Hsp70 proteins in this animal model. As shown before, the expression of Hsp70 is modest and very variable (30) unless the mucosa is under stress (4). Hsp70 expression did not correlate with DSS-induced colitis (Fig. 2G and H). The expression of Hsc70, however, was significantly decreased (69%) in colonocytes under inflammation (Fig. 2G and H). While this result is generally in agreement with a previous report of decreased Hsp70 family proteins in inflammation (18), in that paper the authors found a decrease in Hsp70 but did not report on Hsc70. Hsc70 and Hsp70 are 86% homologous at the amino acid level and are thought to have the same functions, differing only in the regulation of gene expression: Hsc70 is a ubiquitous and constitutive housekeeping gene, while Hsp70 expression is heat shock and stress dependent (11). Therefore, we sought to rule out the possibility that the difference in results between this work and the previous publication may have been due to antibody cross-reactivity, and also to verify whether Hsc70 alone may be sufficient to maintain normal levels of aPKC. To this effect, we repeated the same type of experiments, using Hsp70A/B double-knockout mice. These mice did not show any detectable intestinal phenotype. They responded to DSS treatment just like the wild-type strain. More importantly, they displayed similar levels of active aPKC under control conditions, as measured by pT555. Just like in wild-type animals, Hsc70 expression signficantly decreased in DSS-treated colonocytes (62%) (Fig. 2I and J). Published data (30) indicate that aPKC refolding can be abrogated by immunodepletion of both Hsc and Hsp70 *in vitro* and can be rescued by recombinant Hsp70, but to our knowledge, there are no publications showing rescue with Hsc70 alone. Thus, these results in Hsp70-null animals are also consistent with a model of Hsp70/Hsc70 redundancy for the rescue of aPKC.

TNF-α signaling increases PKCι degradation by abrogating Hsp70/Hsc70 chaperoning activity. A decrease in the steady-state levels of PKCι may be due to a decrease in its synthesis, an increase in its degradation, or both. To test a possible transcriptional effect of proinflammatory signaling, we measured PKCι mRNA by qPCR in TNF-α-treated versus control Caco-2 cells (0.99-fold ± 0.06-fold change for 10 ng/ml TNF-α) (means ± standard deviations [SD]) and in colon epithelial cells isolated from DSS-treated mice versus untreated animals (1.7-fold ± 1.6-fold change). These fold changes were calculated using the $2^{-\Delta\Delta CT}$ method (23). Therefore, the changes were considered not significant in both cultured cells and *in vivo*. To determine PKCι synthesis and degradation, we conducted pulse-chase labeling followed by immunoprecipitation. The synthesis of PKCι determined by a short [^{35}S]methionine/cysteine pulse was indistinguishable in cells treated with 10 ng/ml TNF-α compared to controls (Fig. 3A, ^{35}S, upper panels,

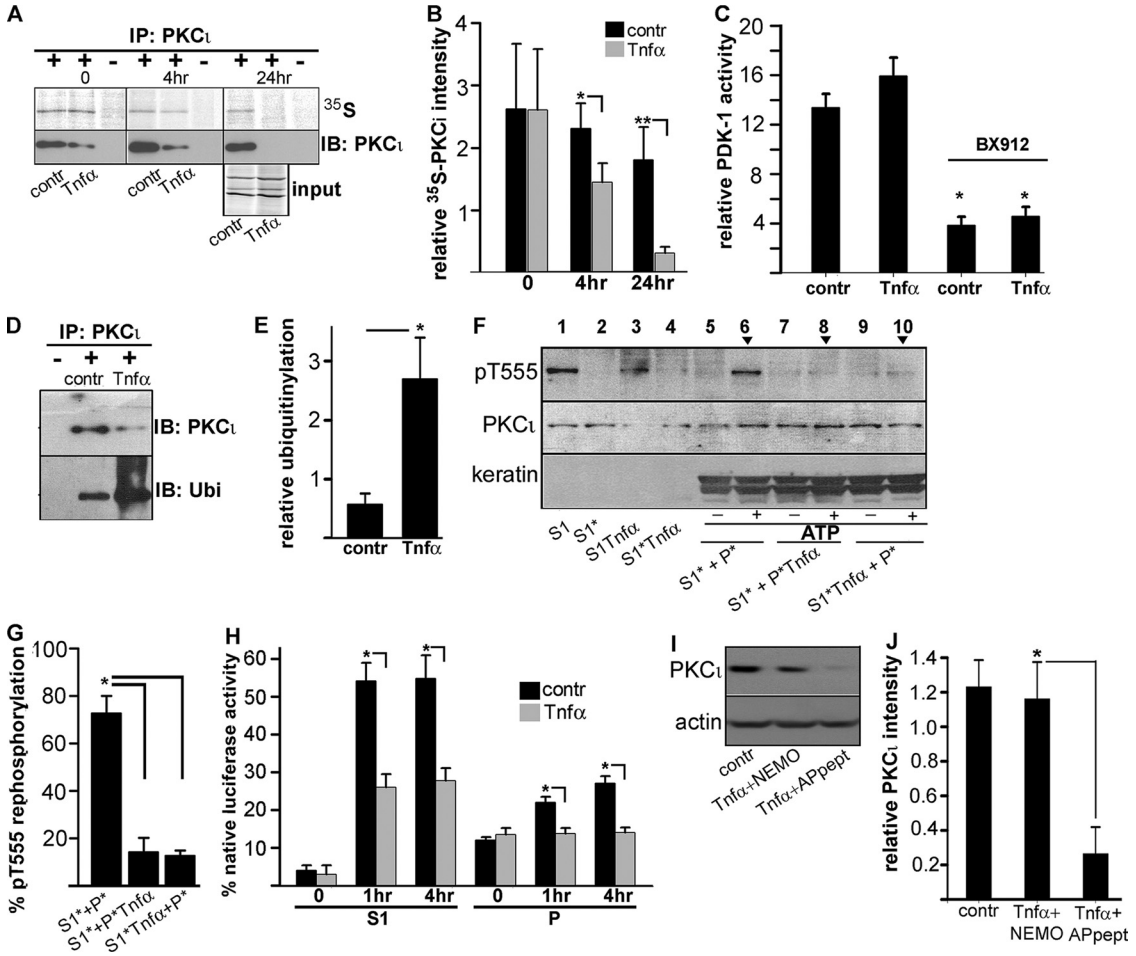

FIG. 3. TNF-α increases aPKC degradation without affecting synthesis or activation. (A) Caco-2 cell monolayers grown on filters for 10 days were incubated with or without (contr) 10 ng/ml TNF-α overnight. The cells were then pulsed with [^{35}S]methionine/cysteine and chased for the indicated times. The Triton-soluble fraction was prepared, immunoprecipitated with anti-PKCι antibody (+) or with nonimmune IgG (−), and analyzed by SDS-PAGE, blotting, and phosphorimaging. The same membranes were probed for total PKCι protein by immunoblotting. A detail of the phosphorimage for the input of the immunoprecipitation mixture after the 24-h chase is included below the immunoblot to show the stability of other, unrelated proteins under similar conditions. (B) Quantification of bands from the experiments shown in panel A. Relative PKCι intensity was calculated by normalizing the amount of PKCι signal to the total signal in the immunoprecipitates. Data represent the means ± SD from three independent experiments. *, $P < 0.05$; **, $P < 0.025$. (C) TNF-α does not affect PDK-1 activity in Caco-2 cells. PDK-1 activity was measured in Caco-2 cells grown to confluence for 10 days on filters. The cells were treated or not (contr) with 10 ng/ml TNF-α overnight, and Triton X-100-soluble fractions S1 (first supernatant) were prepared. In some cases S1 fractions were preincubated with 0.5 μM PDK-1 inhibitor BX-912 for 30 min. Relative kinase activity was normalized per μg of protein. The data are means ± SD from three independent experiments. *, $P < 0.005$ compared to untreated control. (D) TNF-α treatment leads to increased ubiquitinylation of PKCι. Caco-2 cells were cultured and treated with TNF-α as described above and subsequently incubated in 20 μM proteasome inhibitor MG-132 for 6 h. The detergent-solubilized cell lysates were immunoprecipitated with anti-PKCι polyclonal antibody (+) or nonimmune serum (−). Ubiquitinylation of PKCι was detected using an antiubiquitin monoclonal antibody (lower panel, Ubi). The same blot was stripped and reprobed with the anti- PKCι antibody (upper panel). (E) Relative ubiquitinylation was calculated by normalizing the amount of ubiquitin signal to the amount of PKCι in the immunoprecipitates described in panel D. Data represent the means ± SD from three independent experiments (* $P < 0.025$). (F) TNF-α abrogates pT555 PKCι rephosphorylation after activity in reconstitution assays. Fully confluent and differentiated Caco-2 cells were treated or not with 10 ng/ml TNF-α as described abnove and fractionated as described for Fig. 2 into S1 (Triton-soluble fraction, lanes 1 and 3) and P (pellet) fractions. Some fractions were subjected to activity-dependent dephosphorylation, resulting in aPKC in the inactive conformation (S1* [lanes 2 and 4] and P* [data not shown]). Subsequent reconstitution of the S1* fraction with the pellet fraction from control cells (S1*+P*) in the presence of 1 mM ATP for 4 h resulted in rephosphorylation of PKCι (lane 6). Reconstitution of the S1* fraction from control cells with the pellet fraction from TNF-α-treated cells (S1*+P*Tnfα), as well as reconstitution of the S1*Tnfα fraction from TNF-α-treated cells with the pellet fraction from control cells (S1*Tnfα +P*) failed to show PKCι rephosphorylation (lanes 8 and 10). (G) Semiquantitative measurements of the experiments in panel F. The pT555 intensities in experiments similar to that in panel F (lanes 6, 8, and 10 in panel F) were normalized to the total PKCι band density. Data represent the mean ± SD ($n = 3$). *, $P < 0.005$. (H) TNF-α signaling abrogates Hsp/Hsc70 chaperoning activity in Caco-2 cells. Chaperoning activity was measured in the S1 and P fractions of Caco-2 cells (treated with TNF-α or not) by rescue of luminescence in chemically denatured luciferase in the presence of ATP. ATP-dependent activity of the refolded luciferase was measured at the indicated times, and the results are plotted as a percentage of activity of native nontreated luciferase in the presence of S1 or P fractions. Data represent the means ± SD ($n = 3$). *, $P < 0.025$. (I) PKCι downregulation in response to TNF-α treatment is NF-κB dependent. Caco-2 cells grown on filters for 10 days were incubated with 10 ng/ml of TNF-α overnight in the presence of 100 μM control peptide with the antennapedia-derived sequence alone (Tnfα+APpeptide) or 100 μM IKKγ NEMO binding domain inhibitor peptide, including the antennapedia sequence for membrane permeability (Tnfα+NEMO), or without TNF-α (contr). (J) Quantification of the experiments shown in panel I. Relative PKCι intensity was calculated as the ratio of PKCι to actin band densities. The means ± SD from three independent experiments are shown. *, $P < 0.025$.

and 3B, time zero). However, after 4 h of chase we observed a significantly decreased amount of labeled PKCι in the presence of TNF-α. The difference was even more pronounced at the 24-h chase point, where the remaining amount of labeled PKCι in TNF-α-treated cells represented only 17% of that in control cells. In all cases, the total PKCι protein immunoprecipitated and detected by immunoblotting from TNF-α-treated cells was less than in controls, consistent with the results in Fig. 1. As a matter of fact, total PKCι protein decreased after overnight incubation in TNF-α and was almost undetectable after an additional 24 h of incubation (Fig. 3A, IB: PKCι, lower panels). Thus, metabolic labeling experiments revealed a strong effect of TNF-α exposure only on PKCι degradation.

We also tested the possibility that proinflammatory signals affect aPKC activation, and thus the pT555 signal, in addition to its degradation. However, PDK-1 activity was not significantly affected by TNF-α treatment, although it was equally impaired by the PDK-1 inhibitor BX912 (Fig. 3C). Then, considering the results of the pulse-chase studies, we turned our attention to the proteasome degradation pathway. After TNF-α treatment, aPKC ubiquitinylation increased almost 4-fold in the presence of a proteasome inhibitor (Fig. 3D and E). It is known that PKC isoforms in general (14) and aPKC in particular (30) depend on Hsc/Hsp70 protein chaperoning activity to be resphosphorylated and rescued from ubiquitinylation/degradation. We used a previously reported *in vitro* reconstitution assay (30) to determine this rescue activity. As previously reported, when T555-aPKC-dephosphorylated Triton X-100-soluble fractions (S1*) were reconstituted with the T555-aPKC-dephosphorylated intermediate filament pellet (P*) and ATP was restored, the system rephosphorylated T555-aPKC in an Hsp70- and keratin-dependent manner (Fig. 3F, lane 6). However, when either the pellet fractions (P*Tnf) or the detergent-soluble fractions (S1*Tnf) were obtained from TNF-α-treated cells, the rescue significantly failed by 80% (Fig. 3F, lanes 8 and 10, and G). These results indicate that TNF-α treatment severely impairs the aPKC rescue machinery.

TNF-α signaling inhibits Hsc/Hsp70 chaperoning activity. aPKC rescue is dependent on Hsc/Hsp70, and these proteins were present in both the S1 and P fractions of the reconstitution assay shown above, unlike keratins, which are only present in the P fraction (Fig. 1D). Therefore, the fact that S1*Tnf failed to reconstitute aPKC rescue suggested that the chaperone activity in P* may be inhibited by proinflammatory signaling products present in S1*Tnf. Likewise, such a putative inhibition may be retained in the P*Tnf keratin-associated chaperones, despite reconstitution with a "normal" (untreated) S1*. Thus, it seemed reasonable to measure directly the chaperoning activity by using the well-established chemically denatured luciferase refolding assay. Because of the results in the aPKC rescue assay (Fig. 3F), we tested chaperoning activity in both the S1 and the P fractions obtained from TNF-α-treated or untreated cells. In the soluble S1 fractions, ATP-dependent refolding of luciferase was reduced by more than 50% compared to controls, while in the P fractions it was completely absent (Fig. 3H). It must be noted that chaperoning activity was normalized to total protein, which resulted in less Hsc/Hsp70 in the P compared to the S1 fractions (Fig. 1D). These results indicate that decreased steady-state levels of aPKC under inflammatory signaling result from an impaired Hsp70 rescue mechanism with severely decreased chaperoning activity, in addition to decreased Hsc70 expression *in vivo*. Inhibition of Hsp/Hsc70 activity can explain the destabilization of aPKC in Caco-2 cells, where Hsp/Hsc70 protein levels do not change, and in colonocytes *in vivo*, where Hsc70 protein levels decrease but Hsp70 levels are erratic.

To determine whether the effect of TNF-α on PKCι protein expression was also dependent on NF-κB activation, we examined the effect of the IKKγ NEMO binding domain inhibitory peptide, which includes a protein transduction sequence derived from antennapedia to make it membrane permeable. This inhibitory peptide almost completely prevented the decrease in the atypical PKC protein level (Fig. 3I and J), confirming that NF-κB activation is required for the downregulation of PKCι protein expression.

Sustained loss of aPKC activity mimics effects of TNF-α signaling and results in upregulation of MYH9 expression in epithelial cells. To test if loss of aPKC activity phenocopies inflammatory signaling in epithelial cells, we used two systems. First, PKCι was knocked down in Caco-2 cells by using a lentivirus-delivered shRNA followed by puromycin selection. PKCι represents more than 90% of aPKC activity in Caco-2 cells (48), and the knockdown was very effective (Fig. 4A, insert). A second, independent way to specifically block aPKC activity was a prolonged incubation with the myristoylated aPKC pseudosubstrate peptide, which specifically blocks PKCι and PKCζ. Both treatments independently decreased transepithelial electrical resistence (TER) by about 50% (Fig. 4A), a value similar to the effect of a 48-h incubation in TNF-α (26). A similar increase in permeability was also verified in a Caco-2 subclone, C2BB2e, which is generally considered more homogeneous and better polarized than the parental Caco-2 line. In these cells, the anti-aPKC peptide increased the transepithelial flux of fluorescent (fixable) Lucifer yellow CH by more than 2-fold (Fig. 4B). To determine if this flux was paracellular, as a result of more-permeable tight junctions, as opposed to being the result of the dye passing through necrotic cells or holes left by effaced cells, the monolayers were fixed in formaldehyde during the flux. The fixed dye colocalized with the contour of the lateral domains, as determined with fluorescent phalloidin, and was not found inside any cell (Fig. 4C, arrows).

Because myosin II assembly and MLCK expression are considered major effectors of TNF-α signaling in epithelial cells, we tested the status of MLC phosphorylation in Caco-2 cells under PKCι knockdown. We found an increase in phosphorylated MLC (Fig. 4E, upper panel), confirming that MLC phosphorylation is downstream of aPKC. Moreover, we observed an over-4-fold increase in nonmuscle myosin type II heavy chain MYH9 expression (Fig. 4E). Immunolabeling and confocal microscopy of confluent Caco-2 monolayers revealed strong upregulation of MYH9 in the apical domain of PKCι knockdown cells (Fig. 4D). Notably, the other nonmuscle myosin heavy chains MYH10 (Fig. 4D, E, and F) and MYH14 (data not shown) protein levels did not change, which is in agreement with the previously published data about MYH9, but neither MYH10 nor MYH14, playing a role in regulation of epithelial apical junctions (20). Therefore, aPKC downregulation contributes to the accumulation of nonmuscle type II myosin at the apical domain by substantially upregulating one

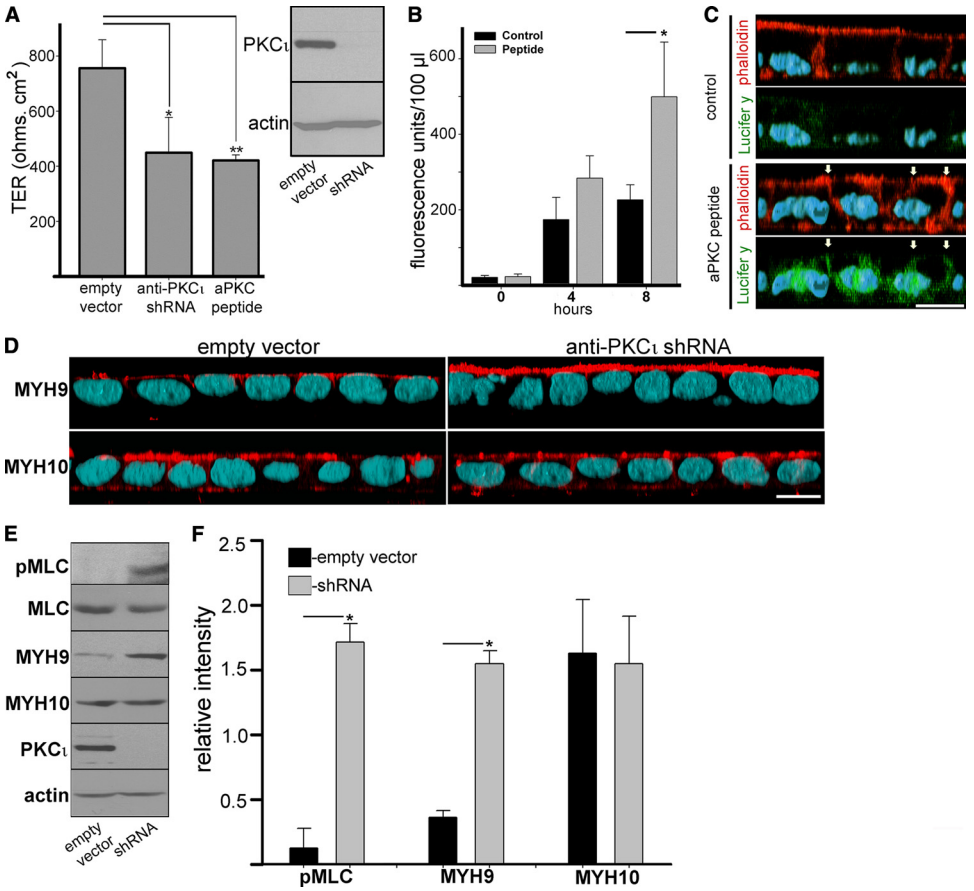

FIG. 4. aPKC knockdown impairs TJ barrier function and upregulates MYH9 expression. Caco-2 cells were transduced with mock lentiviral particles (empty vector) or with particles expressing shRNA anti-PKCι. (A) After puromycin selection, the cells were plated in Snapwell filters, and the TER was measured in Ussing chambers in quintuplicates. A group of filters with mock-transduced cells was also incubated in 50 μM myristoylated aPKC pseudosubstrate peptide, which specifically blocks kinase activity in PKCι and PKCζ. Data are presented as averages ± SD of three independent experiments. *, $P < 0.05$; **, $P < 0.02$. The efficiency of the shRNA-mediated knockdown was determined in parallel monolayers by immunoblotting with anti-total PKCι antibody and found to be >90% (insert). (B) In similar experiments, fully differentiated Caco-2 cells grown on filters were incubated in 50 μM myristoylated aPKC pseudosubstrate peptide for 3 days (peptide) or in phenol red-free medium alone (control). All the cells were supplemented with 0.2 mg/ml Lucifer yellow CH from the apical chamber only (time zero), and 100-μl aliquots of the basal chamber were taken with replacement at the indicated times. (C) In similar experiments, Caco-2 cells (C2BBe clone) were treated or not (control) with myristoylated aPKC pseudosubstrate peptide for 3 days, incubated in Lucifer yellow CH (Lucifer y; green channel) from the apical side for the last 8 h, fixed in formaldehyde, and processed with Alexa 546-phalloidin (red channel) and DAPI (light blue channel). Arrows indicate the position of the lateral membrane. (D) Caco-2 cells transduced with PKCι shRNA or with mock lentivirus (empty vector) were plated on Transwell filters. At 10 days after seeding, the cells were fixed and processed with anti-MYH9 or anti-MYH10 antibodies (red channel) and DAPI (light blue channel). In both panels C and D, the images are three-dimensional reconstructions of confocal stacks shown in the *x-z* plane with the apical side up. Bars, 10 μm. (E) PKCι shRNA-mediated knockdown results in upregulation of MYH9. Caco-2 cells were transduced as described above, but total SDS extracts were analyzed by immunoblotting with the antibodies indicated on the left. (F) Quantification of the results shown in panel E. The bars represent the averages ± STD of the ratio of densitometric values of the bands versus the actin band in the mock-infected (empty vector) group or in PKCι knockdown cells (shRNA) from three independent experiments. *, $P < 0.01$.

of the heavy chains in a mechanism that involves MLC phosphorylation.

TNF-α signaling and inflammation *in vivo* upregulate MYH9 and can be rescued by constitutively active A120E PKCι. Because to our knowledge the upregulation of MYH9 has not been reported in association with proinflammatory signaling, we wanted to verify if it is indeed upregulated under inflammatory conditions *in vivo*. In mouse colonocytes, under the standard DSS treatment described above, MYH9 increased approximately 10-fold (Fig. 5A and B), and the increased signal accumulated at the apical domain (Fig. 5C). Likewise, Caco-2 cells treated with TNF-α for 4 days showed an accumulation of myosin II heavy chain MYH9 at the apical domain (Fig. 5D). MYH10, on the other hand, showed the typical apical junction distribution (Fig. 5D, arrows) but did not change with the TNF-α treatment. A time course of the TNF-α treatment showed that PKCι was abrogated by TNF-α signaling in 24 h, but MYH9 upregulation required 72 h to plateau (Fig. 5E and F). As shown before, MYH10 was not affected by TNF-α. Once again, we found no evidence of apoptosis for these prolongued TNF-α treatments either (Fig. 5E, lower panel).

To test whether aPKC downregulation actually mediates the TNF-α-dependent MYH9 upregulation, Caco-2 cells were

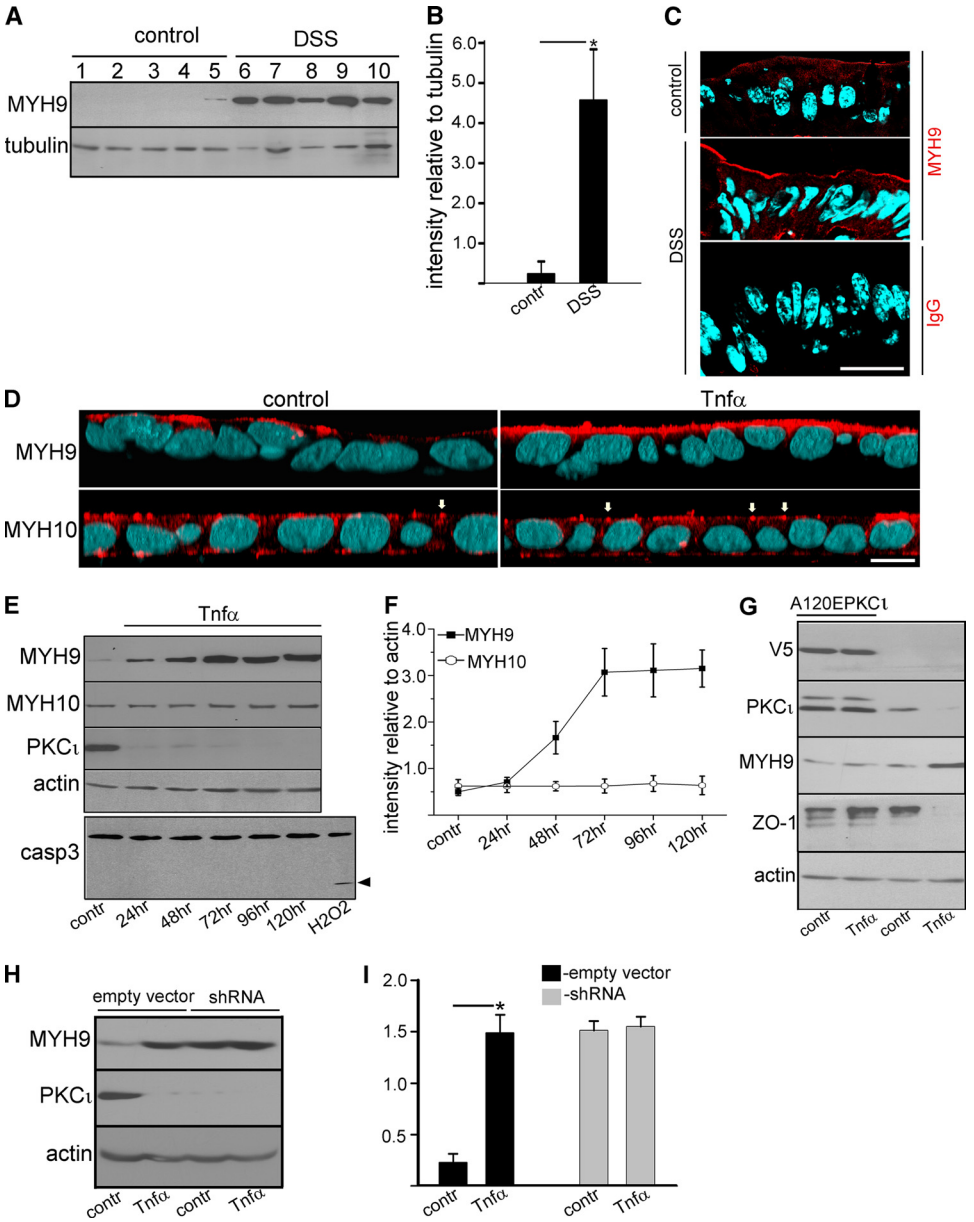

FIG. 5. Proinflammatory signaling upregulates MYH9 expression in intestinal epithelial cells, and the upregulation can be rescued by constitutively active PKCι expression. (A) Colon epithelial cells from five control mice (lanes 1 to 5) and five DSS-treated mice (lanes 6 to 10) were isolated, extracted in SDS, run on an SDS-PAGE gel, and blotted. (B) Quantification of the results shown in panel A. The bars represent the averages ± STD of the ratios of densitometric values of the MYH9 bands versus tubulin bands in the control (contr) or DSS-treated mice (DSS). *, $P < 0.025$. (C) Colons were harvested from control mice or mice with DSS-induced colitis, fixed in 10% trichloroacetic acid, and frozen. Frozen sections were processed with anti-MYH9 antibody (red channel) and counterstained with DAPI (light blue). Control sections were processed with nonimmune IgG at the same dilutions (lower panel). The images are single confocal sections. Bars, 20 μm. (D) Caco-2 cell monolayers grown on filters for 10 days were incubated with or without (contr) 10 ng/ml TNF-α for 96 h (starting at day 6 from seeding). Following the incubation cells were fixed and processed with anti-MYH9 or anti-MYH10 antibodies (red channel). DAPI staining is shown in light blue. The images are three-dimensional reconstructions of confocal stacks shown in the *x-z* plane with the apical side up. Arrows point at cell-cell boundaries. Bar, 10 μm. (E) Caco-2 cells grown on filters for 10 days were treated or not (contr) with 10 ng/ml TNF-α for the indicated periods of time for up to 120 h. After the treatment, SDS extracts were run on SDS-PAGE gels and immunoblotted with the antibodies indicated on the left. The apoptosis level in TNF-α-treated cells was assessed based on caspase-3 cleavage. A positive control of apoptosis was performed by incubating Caco-2 cells in 30 mM H_2O_2 for 2 h (lower panel; the arrowhead indicates cleaved caspase-3). (F) Quantification of the results shown in panel E. The graph shows MYH9 and MYH10 protein expression levels following TNF-α treatment for various periods of time. Each point represents the average ± STD of the ratio of densitometric values of MYH9 or MYH10 bands versus actin bands in the control cells (contr) or in TNF-α-treated cells at different time points. (G) Overexpression of constitutively active PKCι prevents upregulation of MYH9 and downregulation of ZO-1 in TNF-α-treated Caco-2 cells. Caco-2 cells were transduced with lentiviral particles carrying a V5-tagged constitutively active PKCι mutant (A120EPKCι). After blasticidin selection, the cells were plated on Transwell filters and treated or not (contr) with 10 ng/ml of TNF-α for 72 h. Following the incubation the cells were extracted with SDS, run on SDS-PAGE gels, and blotted. The expression of the A120EPKCι mutant was verified using anti-V5 antibody. (H) PKCι knockdown and TNF-α signaling are not additive for the expression of MYH9. Caco-2 cells transduced with PKCι shRNA or with mock lentivirus (empty vector) grown on filters for 10 days were incubated with or without (contr) 10 ng/ml TNF-α for 72 h (starting at day 7 from seeding). Following the incubation the cells were extracted with SDS, run on SDS-PAGE gels, and blotted. (I) Quantification of the results shown in panel H. The bars represent the averages ± STD of the ratios of densitometric values of the bands versus the actin band in the mock-infected control (empty vector) or in PKCι knockdown cells (shRNA) from three independent experiments. *, $P < 0.025$.

transduced with lentiviral particles expressing the constitutively active A120E PKCι. The cells were selected to ensure homogeneous expression and then subjected or not (controls) to TNF-α treatment. Parallel monolayers of nontransduced cells were treated similarly. In the cells not expressing the active PKCι mutant, the endogenous kinase was downregulated under TNF-α signaling and MYH9 was upregulated. In transduced cells, the PKCι levels were about 3-fold higher than in nontranduced cells, indicating a moderate level of overexpression. In these cells TNF-α treatment did not cause a substantial decrease in the PKCι levels. More importantly, MYH9 was not upregulated under TNF-α signaling, indicating that the overexpression of PKCι rescued this effect. It was previously demonstrated that the TNF-α-induced increase in TJ permeability is associated with downregulation of ZO-1 protein expression (26). In agreement with these published data, there was a profound decrease in the amount of ZO-1 protein after TNF-α treatment in nontransduced Caco-2 cells. In contrast, TNF-α did not affect ZO-1 expression in cells with constitutively active PKCι (Fig. 5G), indicating that PKCι can rescue TNF-α-induced ZO-1 downregulation.

To further confirm the involvement of PKCι in TNF-α-mediated proinflammatory signaling, we tested whether TNF-α treatment of cells lacking atypical PKC yielded an additional effect on MYH9 upregulation. As shown in Fig. 5H and I, TNF-α treatment did not lead to a significant additional increase in MYH9 expression in PKCι shRNA-infected cells. This finding suggests that lack of atypical PKC is sufficient to mimic the TNF-α effect on MYH9.

DISCUSSION

The results in this work reveal four novel conclusions. (i) Proinflammatory signals can downregulate the expression levels of aPKC in its active conformation by 1 order of magnitude, thus disrupting the polarity complex in an NF-κB-dependent manner. (ii) Changes in the expression or activity of aPKC of similar magnitude are sufficient to perturb the barrier function in intestinal epithelia. It is conceivable that similar effects may apply for the expression of aPKC in other tissues. Loss of barrier function in epithelia is a dire consequence of inflammatory processes. (iii) Not only are Hsp proteins downregulated *in vivo*, but also their intrinsic activity is abrogated under TNF-α signaling. (iv) There is an upregulation of the myosin II heavy chain type A (MYH9), which is specifically dependent on aPKC downregulation and phenocopies the TNF-α-induced accumulation of myosin II (Fig. 5). Conversely, the fact that a basal level of MYH9 is still detectable in the presence of constitutively active PKCι (Fig. 5G) only resembles the findings that steady-state levels of MLC are still observable under MLCK knockout conditions (9). In other words, posttranslational effects on assembly are not expected to affect basal levels of protein (MYH9 or MLC) expression.

In IBD, epithelial barrier dysfunction is considered an essential factor, leading to mucosal lesions and the chronicity of the disease (8). Accordingly, persistence of high permeability in the intestinal epithelium is a good predictor of recurrence in relapsing IBD patients (12, 49). Recently, genome studies have identified mutations in transcription factors controlling the expression of TJ and adherens junction components as predisposing for ulcerative colitis (3). There is no evidence linking any mutation in atypical PKC as a predisposing factor for IBD. The aPKC mechanism described here, along with the MLCK upregulation reported by other laboratories, are therefore effectors rather than causes of the inflammatory response in epithelia.

The MLCK upregulation has been considered the major response to proinflammatory signaling in epithelial cells. The intestine-specific long MLCK conditional null mouse is protected from intestinal inflammation induced by anti-CD3 antibody over very short periods of time (3 h) (9). The effects of aPKC downregulation are much slower and can be demonstrated only after 48 h. The distributions of active MLCK in those studies, on the other hand, are indistiguishable from the distribution of MYH9 in our study, suggesting that both accumulate together under the entire apical domain. Therefore, both mechanisms can be complementary in the context of chronic inflammation. The simplest interpretation of the data presented here is that aPKC is interposed in the pathway downstream of NF-κB and upstream of MLC phosphorylation. Whether or not it is synergistic with MLCK upregulation remains to be determined.

These results do not negate other signaling pathways that may contribute to remove or degrade individual TJ components under the effects of proinflammatory signaling (21, 38) and which may be synergistic. Importantly, aPKC destabilization cannot be predicted on the basis of gene expression microarrays or genetic studies. In turn, this novel mechanism may provide unexpected opportunities for therapeutic intervention. In fact, there are other potential consequences of a profound downregulation of aPKC during inflammation that have not been analyzed here but which deserve further studies. Within the polarity complex, PAR3 is known to be phosphorylated by aPKC (27, 33), and it is also affected by TNF-α signaling (Fig. 1G), opening several possible consequences for inflammatory signaling that remain to be explored. aPKC is also important for the apical exclusion of endocytosis adaptor Numb (7) and the activation of apical ezrin in early epithelial differentiation (48). An additional, and perhaps more significant, aspect of the observations in this work arises from the functional inhibition and downregulation of Hsp/Hsc70 proteins. These chaperones are essential for maintaining several clients, including kinases involved in various signaling pathways. Thus, it is possible that the Hsp/Hsc70 defect downstream of the TNF receptor and Nf-κB signaling in the context of inflammation may set novel pathophysiological paradigms for epithelial function.

ACKNOWLEDGMENTS

We thank Richard Rotundo for critically reviewing the manuscript and for help with the metabolic labeling experiments and Yolanda Menendez for excellent technical assistance.

This work was supported by grants R01-DK076652 and R01-DK087359 to P.J.S.

REFERENCES

1. **Andoh, A., et al.** 2008. Mucosal cytokine network in inflammatory bowel disease. World J. Gastroenterol. **14:**5154–5161.
2. **Baker, O. J., et al.** 2008. Proinflammatory cytokines tumor necrosis factor-alpha and interferon-gamma alter tight junction structure and function in the rat parotid gland Par-C10 cell line. Am. J. Physiol. Cell Physiol. **295:**C1191–C1201.
3. **Barrett, J. C., et al.** 2009. Genome-wide association study of ulcerative colitis

identifies three new susceptibility loci, including the HNF4A region. Nat. Genet. **41:**1330–1334.
4. **Baumler, M. D., D. W. Nelson, D. M. Ney, and G. E. Groblewski.** 2007. Loss of exocrine pancreatic stimulation during parenteral feeding suppresses digestive enzyme expression and induces Hsp70 expression. Am. J. Physiol. Gastrointest. Liver Physiol. **292:**G857–G866.
5. **Bruewer, M., et al.** 2003. Proinflammatory cytokines disrupt epithelial barrier function by apoptosis-independent mechanisms. J. Immunol. **171:**6164–6172.
6. **Bruewer, M., S. Samarin, and A. Nusrat.** 2006. Inflammatory bowel disease and the apical junctional complex. Ann. N. Y. Acad. Sci. **1072:**242–252.
7. **Casanova, J. E.** 2007. PARtitioning Numb. EMBO Rep. **8:**233–235.
8. **Cario, E.** 2008. Barrier-protective function of intestinal epithelial Toll-like receptor. Mucosal Immunol. **1**(Suppl. 1)**:**S62–S66.
9. **Clayburgh, D. R., et al.** 2005. Epithelial myosin light chain kinase-dependent barrier dysfunction mediates T cell activation-induced diarrhea in vivo. J. Clin. Invest. **115:**2702–2715.
10. **Cooper, H. S., S. N. Murthy, R. S. Shah, and D. J. Sedergran.** 1993. Clinicopathologic study of dextran sulfate sodium experimental murine colitis. Lab. Invest. **69:**238–249.
11. **Daugaard, M., M. Rohde, and M. Jäättelä.** 2007. The heat shock protein 70 family: highly homologous proteins with overlapping and distinct functions. FEBS Lett. **581:**3702–3710.
12. **D'Incà, R., et al.** 1999. Intestinal permeability test as a predictor of clinical course in Crohn's disease. Am. J. Gastroenterol. **94:**2956–2960.
13. **Fries, W., C. Muja, C. Crisafulli, S. Cuzzocrea, and E. Mazzon.** 2008. Dynamics of enterocyte tight junctions, effect of experimental colitis and two different anti-TNF strategies. Am. J. Physiol. Gastrointest. Liver Physiol. **294:**G938–G947.
14. **Gao, T., and A. C. Newton.** 2006. Invariant Leu preceding turn motif phosphorylation site controls the interaction of protein kinase C with Hsp70. J. Biol. Chem. **281:**32461–32468.
15. **Goldstein, B., and I. G. Macara.** 2007. The PAR proteins, fundamental players in animal cell polarization. Dev. Cell **13:**609–622.
16. **Gould, C. M., and A. C. Newton.** 2008. The life and death of protein kinase C. Curr. Drug Targets **9:**614–625.
17. **Holgate, S. T.** 2007. Epithelium dysfunction in asthma. J. Allergy Clin. Immunol. **120:**1233–1244.
18. **Hu, S., et al.** 2007. Translational inhibition of colonic epithelial heat shock proteins by IFN-gamma and TNF-alpha in intestinal inflammation. Gastroenterology **133:**1893–1904.
19. **Ikenouchi, J., K. Umeda, S. Tsukita, M. Furuse, and S. Tsukita.** 2007. Requirement of ZO-1 for the formation of belt-like adherens junctions during epithelial cell polarization. J. Cell Biol. **176:**779–786.
20. **Ivanov, A. I., et al.** 2007. A unique role for nonmuscle myosin heavy chain IIA in regulation of epithelial apical junctions. PLoS One **8:**e658.
21. **Koch, S., and A. Nusrat.** 2009. Dynamic regulation of epithelial cell fate and barrier function by intercellular junctions. Ann. N. Y. Acad. Sci. **1165:**220–227.
22. **Lang, W., H. Wang, L. Ding, and L. Xiao.** 2004. Cooperation between PKC-alpha and PKC-epsilon in the regulation of JNK activation in human lung cancer cells. Cell Signal **16:**457–467.
23. **Livak, K. J., and T. D. Schmittgen.** 2001. Analysis of relative gene expression data using real-time quantitative PCR and the 2(-ΔΔC(T)) method. Methods **25:**402–408.
24. **Lu, Z., and D. M. Cyr.** 1998. Protein folding activity of Hsp70 is modified differentially by the hsp40 co-chaperones Sis1 and Ydj1. J. Biol. Chem. **273:**27824–27830.
25. **Ma, T. Y., M. A. Boivin, D. Ye, A. Pedram, and H. M. Said.** 2005. Mechanism of TNF-α modulation of Caco-2 intestinal epithelial tight junction barrier: role of myosin light-chain kinase protein expression. Am. J. Physiol. Gastrointest. Liver Physiol. **288:**G422–G430.
26. **Ma, T. Y., et al.** 2004. TNF-α-induced increase in intestinal epithelial tight-junction permeability requires NF-κB activation. Am. J. Physiol. Gastrointest. Liver Physiol. **286:**G367–G376.
27. **Macara, I. G.** 2004. Parsing the polarity code. Nat. Rev. Mol. Cell Biol. **5:**220–231.
28. **Maloy, K. J.** 2008. The interleukin-23/interleukin-17 axis in intestinal inflammation. J. Intern. Med. **263:**584–590.
29. **Mankertz, J., and J. D. Schulzke.** 2007. Altered permeability in inflammatory bowel disease, pathophysiology and clinical implications. Curr. Opin. Gastroenterol. **23:**379–383.
30. **Mashukova, A., A. S. Oriolo, F. A. Wald, and P. J. Salas.** 2009. Rescue of atypical protein kinase C in epithelia by the cytoskeleton and Hsp70 family chaperones. J. Cell Sci. **122:**2491–2503.
31. **Melgar, S., et al.** 2008. Validation of murine dextran sulfate sodium-induced colitis using four therapeutic agents for human inflammatory bowel disease. Intl. Immunopharmacol. **8:**836–844.
32. **Mizuno, K., et al.** 2003. Self-association of PAR-3-mediated by the conserved N terminal domain contributes to the development of epithelial tight junctions. J. Biol. Chem. **278:**31240–31250.
33. **Morais-de-Sá, E., V. Mirouse, and D. St. Johnston.** 2010. aPKC phosphorylation of Bazooka defines the apical/lateral border in Drosophila epithelial cells. Cell **141:**509–523.
34. **Newton, A. C.** 2003. Regulation of the ABC kinases by phosphorylation, protein kinase C as a paradigm. Biochem. J. **370:**361–371.
35. **Noguchi, M., N. Hiwatashi, Z. Liu, and T. Toyota.** 1998. Secretion imbalance between tumour necrosis factor and its inhibitor in inflammatory bowel disease. Gut **43:**203–209.
36. **Pinto, M., et al.** 1983. Enterocyte-like differentiation and polarization of the human colon carcinoma cell line Caco-2 in culture. Biol. Cell **47:**323–330.
37. **Rose, L. S., and K. J. Kemphues.** 1998. Early patterning of the C. elegans embryo. Annu. Rev. Genet. **32:**521–545.
38. **Roy, P. K., F. Rashid, J. Bragg, and J. A. Ibdah.** 2008. Role of the JNK signal transduction pathway in inflammatory bowel disease. World J. Gastroenterol. **14:**200–202.
39. **Sandoval, K. E., and K. A. Witt.** 2008. Blood-brain barrier tight junction permeability and ischemic stroke. Neurobiol. Dis. **32:**200–219.
40. **Steinert, P., R. Zackroff, M. Aynardi-Whitman, and R. D. Goldman.** 1982. Isolation and characterization of intermediate filaments. Methods Cell Biol. **24:**399–419.
41. **St. Johnston, D., and J. Ahringer.** 2010. Cell polarity in eggs and epithelia: parallels and diversity. Cell **141:**757–774.
42. **Suzuki, A., and S. Ohno.** 2006. The Par aPKC system, lessons in polarity. J. Cell Sci. **119:**979–987.
43. **Suzuki, A., et al.** 2002. aPKC kinase activity is required for the asymmetric differentiation of the premature junctional complex during epithelial cell polarization. J. Cell Sci. **115:**3565–3573.
44. **Turner, J. R.** 2006. Molecular basis of epithelial barrier regulation: from basic mechanisms to clinical application. Am. J. Pathol. **169:**1901–1909.
45. **Umeda, K., et al.** 2006. ZO-1 and ZO-2 independently determine where claudins are polymerized in tight-junction strand formation. Cell **126:**741–754.
46. **Utech, M., et al.** 2005. Mechanism of IFN-gamma-induced endocytosis of tight junction proteins: myosin II-dependent vacuolarization of the apical plasma membrane. Mol. Biol. Cell **16:**5040–5052.
47. **Vicente-Manzanares, M., X. Ma, R. S. Adelstein, and A. R. Horwitz.** 2009. Non-muscle myosin II takes centre stage in cell adhesion and migration. Nat. Rev. Mol. Cell Biol. **10:**778–790.
48. **Wald, F. A., et al.** 2008. Atypical protein kinase C (iota) mediates local ezrin activation in the apical domain of intestinal epithelial cells. J. Cell Sci. **121:**644–654.
49. **Wyatt, J., H. Vogelsang, W. Hübl, T. Waldhöer, and H. Lochs.** 1993. Intestinal permeability and the prediction of relapse in Crohn's disease. Lancet **341:**1437–1439.
50. **Ye, D., I. Ma, and T. Y. Ma.** 2006. Molecular mechanism of tumor necrosis factor-alpha modulation of intestinal epithelial tight junction barrier. Am. J. Physiol. Gastrointest. Liver Physiol. **290:**G496–G504.